Int. J. Heat Mass Transfer. Vol. 19, pp. 737–750. Pergamon Press 1976. Printed in Great Britain

SECONDARY MEAN MOTIONS ARISING IN A BUOYANCY INDUCED FLOW

T. AUDUNSON† and B. GEBHART‡

(*Received* 7 *May* 1975 *and in revised form* 3 *November* 1975)

Abstract—The paper presents numerical calculations of the growth and non-linear interaction of two dimensional and transverse disturbances in a natural convection boundary layer flow adjacent to a vertical flat plate. We find that finite amplitude effects result in a double longitudinal mean secondary vortex system. At certain spanwise positions and, for particular phases of the primary wave, this highly organized longitudinal circulation causes an alternate spanwise thinning and thickening of the boundary region and resultant steepening and flattening of the base flow velocity profile. Measurements of the response of the flow to controlled two-dimensional streamwise disturbances, modulated by a transverse standing wave also show similar characteristics and that, in fact, the two disturbance features are and remain locked together at a small phase difference. Experimentally determined transition conditions thus correspond very closely to flows in which this analysis finds large vortex motions.

NOMENCLATURE

a, perturbation amplitude;
c_p, specific heat;
$F(\eta)$, similarity stream function for the base flow;
g, gravitational acceleration;
G^*, flux Grashof number $= 5\sqrt[5]{(gqx^4/k^25)}$;
$H(\eta)$, similarity temperature function for the base flow;
$\mathbf{i}$, unit vector in the vertical (x) direction;
i, unit coordinate in the complex plane;
$\mathbf{k}$, thermal conductivity;
p, fluid pressure;
Pr, Prandtl number $= \nu/\alpha$;
$\mathbf{q}$, (u, v, w)—velocity vector;
q, wall heat flux;
t, fluid temperature;
t_∞, ambient temperature;
T, characteristic temperature;
U, characteristic velocity;
u, velocity in the x-direction;
v, velocity in the y-direction;
w, velocity in the z-direction;
x, coordinate in the principal flow direction;
y, coordinate perpendicular to the surface;
z, coordinate in the transverse direction.

Greek symbols

α, complex disturbance wave number $= \alpha_r + i\alpha_i$;
α, thermal diffusivity;
β, complex disturbance frequency $= \beta_r + i\beta_i$;
δ, characteristic boundary layer thickness $= 5x/G^*$;
η, similarity variable $= (y/\delta)$;
$\phi(y)$, velocity disturbance function;
λ, strength of transverse disturbance;
μ, strength of two dimensional disturbance;
$\psi(x, y, z)$, velocity stream function;
ρ, fluid density;
ν, kinematic viscosity;
τ, time;
θ, transverse wave number.

INTRODUCTION

LINEAR stability theory has greatly increased our understanding of the initial growth of disturbances in laminar flows. Many of the predictions for external flows are strongly supported by experimental evidence. Among the earliest such results were those of Schubauer and Skramstad [1] for forced flow. For natural convection flow along a vertical flat surface, stability theory has been corroborated by the experiments of Ćolak-Antić [20], Polymeropolos and Gebhart [3], Knowles and Gebhart [4], and Dring and Gebhart [2]. The predictions of very sharp frequency filtering have been extensively supported by experimental evidence, Godaux and Gebhart [5] and Jaluria and Gebhart [6]. For line scource plumes and for natural convection flow over horizontal or slightly inclined flat surfaces, Pera and Gebhart [7, 8] have reported qualitative agreement between experiment and stability calculations. One may conclude therefore, that the general idea of analyzing stability by superimposing a small oscillating disturbance on a flow, and following its growth downstream, is a reasonable initial approach for buoyancy induced flows.

However, as the amplitude of a disturbance is considered finite, nonlinear mechanisms arise. These are of two kinds. One is the effect of Reynolds stresses in producing a redistribution of momentum in the boundary layer through changes in the mean flow. This may change the rate of energy transport to disturbances. The other is the possibility of generating higher harmonics. Possible effects of higher harmonics on the energy transfer to disturbances are more difficult to conjecture.

For the flow considered here, there is now a fair amount of detailed knowledge concerning the growth

†River and Harbour Laboratory, Trondheim, Norway.
‡Parker Engineering, State University of New York, NY 14214, U.S.A.

of small disturbances. Recent summaries of the present knowledge are given by Gebhart [9, 10]. Although the flow amplifies a broad spectrum of frequencies downstream, both calculations and experiment indicate that a very narrow band is much more rapidly amplified. As a result, almost all disturbance energy is concentrated into a single frequency downstream, i.e. at increasing local Grashof numbers. These disturbances are known to lead directly to the short random bursts of large amplitude which convert the flow to turbulence, see Mollendorf and Gebhart [11], Godaux and Gebhart [5], Jaluria and Gebhart [6].

New measurements have shown, as we would expect, that the breakdown to turbulence is not sudden but is rather a process wherein three-dimensional temporal bursts become more frequent and larger downstream. The observations of Lock and Trotter [12] suggest this, and the very detailed measurements during transition itself by Godaux & Gebhart [5] and Jaluria and Gebhart [6] put the matter in quantitative perspective.

Considering the relative importance of two dimensional and transverse disturbances, much evidence indicates that the former are first unstable downstream, i.e. at a smaller local Grashof number. Direct observations have corroborated this. However, even these results suggest that oblique waves will also be amplified and that some appreciable band of frequency is highly amplified, Hieber and Gebhart [13].

The observed three dimensional nature of bursts, and also of turbulent flow, suggest that three dimensional effects precede transition.

In the earliest study, in air, Eckert and Soehngen [14] detected isolated turbulent spots being convected downstream. However, interferometer visualization precluded any detailed assessment of three dimensional effects. Eckert *et al.* [15], using smoke filaments, observed both longitudinal and transverse vortices. The initial part of the disturbance was mainly two dimensional. Three dimensional effects became increasingly evident as transition was approached. Fujii [16] and Fujii *et al.* [17] used the flow visualization techniques of dye injection, shadograph and Schlieren. The observations were in water and in oils, along a vertical cylinder. It was concluded that transition takes place via the formation of a double row transverse vortex system, i.e. with axis perpendicular to the flow direction and parallel to the surface. Since the diameter of the cylinder was of the order of the wavelength of the disturbance, the observations and conclusions may be limited to that geometry. Szewczyk [18] studied instability and transition in convection along a flat vertical plate in water using a dye for visualization. Transverse vorticity components were again reported. The transition to turbulence was explained in terms of vortex loop formation, similar to the mechanism suggested by Hama [19] for forced flow. Ćolak-Antić [20] used a hot wire to measure the convection of controlled disturbances in air. Although a transverse velocity component was detected, no definite conclusions were drawn concerning the mechanism of transition. We shall have occasion to refer to some other more recent experiments at later stage. However, it is important to note here that for all of the previous data for which we could determine disturbance frequencies, the dominant frequency agreed very closely with that which has been calculated from linear stability theory to be most highly amplified.

Thus, the sequence to transition appears now to be the concentration of almost all disturbance energy into essentially a single frequency two-dimensional disturbance. This is followed by non-linear growth, in conjunction with transverse disturbances, to generate secondary mean motions. The analysis given here attempts to assess first, how the nature of resulting secondary mean flows depend on the local base flow condition, and second, how these secondary flows might differently affect the mean flow.

ANALYSIS

The analysis postulates a two-dimensional disturbance, modulated by a standing transverse disturbance. Crucial questions in the model are the relative amplitudes and wavelengths of these two disturbance components and more important, their relative phase and velocities of propagation downstream.

Our calculations vary the relative amplitude of the two disturbance components. The measurements of Jaluria and Gebhart [6] just ahead of transition resulting from naturally occurring disturbances, indicate that the two wavelengths were comparable in that circumstance. We suppose that their relation depends upon a number of subtle aspects of the particular environment in which the flow is led toward transition. We assume them to be equal.

Concerning propagation velocities, Benny and Lin [21] and Benny [22, 23] assumed them equal for a zero pressure gradient forced flow boundary layer. Stuart [24] has shown that they are not, near the neutral curve, and therefore, presumably not in the amplified region beyond. Similar objections to the assumption of synchronization of two and three dimensional waves are also given by Hocking *et al* [25].

However, there is abundant reason from recent experiment to believe that the velocities of the two disturbance components are nearly the same over a long distance in this highly filtered flow. Jaluria and Gebhart [26] found them to be so in their detailed measurements of controlled disturbance propagation. This kind of evidence is best seen in Fig. 1, where we have plotted, side-by-side, the periodic streamwise disturbance component and the spanwise component, each measured at various local values of G^* in the range from 350 to 545. The two disturbance components are clearly locked together at a small phase difference, which varies from 0.2 to 0.3 of a cycle, with an average value of 0.25 for these data.

The above phase difference may not, in fact, be natural in the sense of the response of a flow to naturally occurring three dimensional disturbances. This disturbance was introduced by a spanwise ribbon parallel to the plate, vibrated normal thereto. The ribbon had equally spaced spanwise sections of 0.125

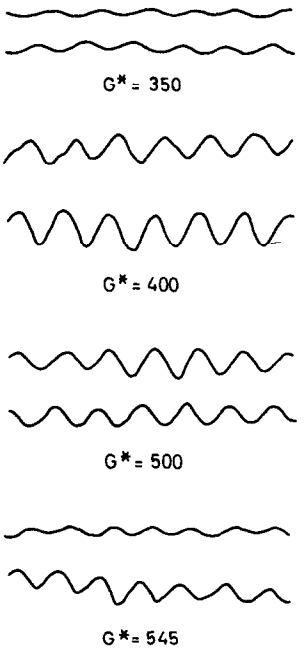

FIG. 1. Two dimensional and transverse velocity disturbances vs time as measured at various downstream locations G^*, as indicated. Upper signal for each G^* is the transverse one.

and 0.0375 in height (i.e. parallel to the flow direction), each of 0.5 in spanwise length. Ribbon amplitude was 0.003 in. Jaluria and Gebhart did not measure the resulting phase relation of the streamwise and transverse disturbances immediately downstream of the ribbon. They were too small, given the noise level. However, consideration of fluid response to such an input suggests that transverse maxima would follow the two dimensional ones. It is fluid motion transversely away from ribbon regions of greater height which causes the transverse modulation. Propagation and dimensional argument both suggest the order of a quarter period lag. More details of this kind of experiment, which also produced the results in Figs. 14–16, are given in the above reference.

We, therefore, make the empirical assumption that the velocities are the same, for the great attendant simplicity this affords. The physical picture of the disturbances, is two dimensional crests, being convected downstream, in phase with a spanwise modulation of their amplitude.

In the analysis, nonlinear effects are retained in the disturbance equations. The basic flow is that induced adjacent to a vertical, uniform-heat-flux surface, in air. Solutions for the first perturbation from linear theory are obtained numerically for several different values of local Grashof number and disturbance frequency, for local conditions from near neutral to highly amplified. The emphasis is on nonlinear effects and their consequences. In the light of new data, briefly considered here, these solutions lead to significant detailed insights concerning the phenomena which lead a laminar flow into transition.

The equations and formulation

Finite amplitude effects are evaluated by setting up a systematic perturbation of linear stability theory. This theory, applied to buoyancy induced flow may be found in adequate detail, e.g. in Hieber and Gebhart [13].

The non-linear interaction of the solutions to the homogeneous Orr–Sommerfeld equations become the driving functions for the first perturbation from linearized analysis. This induced secondary flow may be divided into a secondary mean flow and a second harmonic oscillation. We will consider only the former here.

The equations of transport are written as:

$$\frac{\partial}{\partial\tau}\mathbf{q}+\mathbf{q}\cdot\nabla\mathbf{q} = -\frac{1}{\rho}\nabla p+\nu\nabla^2\mathbf{q}-(i\mathbf{g}\rho)\frac{1}{\rho}$$

$$\rho c_p\left(\frac{\partial t}{\partial\tau}+\mathbf{q}\cdot\nabla t\right)=k\nabla^2 t \qquad (1)$$

$$\nabla\cdot\mathbf{q}=0.$$

The Boussinesq approximation $\Delta\rho/\rho \ll 1$ will be invoked, and the quantities $\mathbf{q}$, t and p are expanded as a perturbation series of the form

$$\mathbf{q}=\mathbf{q}^{(0)}+a\mathbf{q}^{(1)}+a^2\mathbf{q}^{(2)}+$$

$$p=p^{(0)}+ap^{(1)}+a^2p^{(2)}+$$

$$t=t^{(0)}+at^{(1)}+a^2t^{(2)}+$$

where

$$\mathbf{q}^{(n)}=(u^{(n)},v^{(n)},w^{(n)}).$$

The superscript (0) refers to the undisturbed steady laminar flow. Note that $p^{(0)}$ becomes simply the hydrostatic pressure in first order boundary layer theory. The superscript (1) refers to the primary oscillation, etc. and the symbol a is used to denote a perturbation amplitude. For given basic flow, $\mathbf{q}^{(0)}=u^{(0)}(y,0,0)$ and $t^{(0)}=t^{(0)}(y,0,0)$, under the parallel flow assumption. We will use as the basic flow that generated adjacent to a vertical flat surface which dissipates a constant and uniform surface heat flux. This solution was given by Sparrow and Gregg [27] and is the configuration we find most convenient for experiment.

We will consider perturbations up to and including the terms of order a^2 and are particularly interested in the induced second order mean motion.

In actual flows we expect that two-dimensional features of disturbances will first be prominent. Transverse effects will become important further downstream. We assume here that this occurs while the disturbances are still in the linear domain. In forced flow there is strong experimental support for this conjecture in the measurements of Klebanoff *et al.* [28] which show a three-dimensional warping of the mean velocity profile well before transition. In natural convection the qualitative observations of Eckert *et al.* [15], and of Ćolak-Antić [20] suggest this. The measurements of Jaluria and Gebhart [26] with controlled three-dimensional disturbances indicate downstream amplification of transverse disturbance amplitude at G^* values well below the non-linear range.

Therefore, we include both two-dimensional and transverse components in the linear perturbation. We also assume that the transverse disturbance is a standing sinusoidal wave in the spanwise direction. The postulated forms are:

$$u^{(1)}(x, y, z, \tau) = \lambda u_1^{(1)}(y) \cos \theta z \, e^{i(\alpha_1 x - \beta_1 \tau)} + \mu u_2^{(1)}(y) e^{i(\alpha_2 x - \beta_2 \tau)} + \lambda u_1^{(1)*}(y) \cos \theta z \, e^{-i(\alpha_1^* x - \beta_1^* \tau)} + \mu u_2^{(1)*}(y) e^{-i(\alpha_2^* x - \beta_2^* \tau)}. \quad (2)$$

Subscripts 1 and 2 identify the transverse and two-dimensional constituents, respectively. The asterisk indicates complex conjugate. Disturbance frequency and wavelength are $\beta_r/2\pi$ and $2\pi/\alpha_r$, where the subscript r refers to the real parts. The constants λ and μ, which indicate the relative strength of the transverse and two-dimensional disturbances, are assumed real. Thus they are taken to be in phase. This is a reasonable approximation of observations discussed above.

Following the notation of Sparrow and Gregg for the uniform flux surface condition, the characteristic velocity (U), temprature (T), length (δ) and similarity variable η are:

$$U = \frac{\nu}{5x} G^{*2}, \quad T = \frac{q}{k}\delta, \quad \delta = \frac{5x}{G^*}, \quad \eta = \frac{y}{\delta}. \quad (3)$$

Dimensional and non-dimensional quantities are not distinguished here except when both appear in the same expression. Then the dimensional one will be identified with a tilde.

The base flow and two-dimensional disturbance are written as:

$$\psi^{(0)}(x, y, z) = \nu G^* F(\eta)$$
$$\psi^{(1)}(x, y, z) = \phi_2(y) e^{i(\alpha_2 x - \beta_2 \tau)}$$

so that

$$u^{(0)} = \frac{\partial \psi^{(0)}}{\partial y} \quad \text{and} \quad v^{(0)} = -\frac{\partial \psi^{(0)}}{\partial x} \quad (4)$$

and similarly

$$u_2^{(1)} = \frac{\partial \psi^{(1)}}{\partial y} e^{-i(\alpha_2 x - \beta_2 \tau)} \quad \text{and}$$

$$v_2^{(1)} = -\frac{\partial \psi^{(1)}}{\partial x} e^{-i(\alpha_2 x - \beta_2 \tau)}$$

For the transverse part of the general disturbance we introduce the following definition for the velocity component normal to the surface:

$$v_1^{(1)} = -i\alpha_1 \phi_1(y). \quad (5)$$

The temperature distribution of the base flow is expressed as:

$$\frac{\tilde{t} - \tilde{t}_\infty}{\tilde{T}} = H(\eta). \quad (6)$$

The disturbance temperatures are defined as in (2).

To conserve space the governing equations for the base flow and for the 2-D and 3-D primary disturbance amplitude functions will not be reproduced here. One may only mention that they are of the usual coupled Orr–Sommerfeld form. The reader may consult Audunson [29] for further details.

Secondary flows

The mean seeond order disturbance induced by primary disturbance interactions, at this order, is a downstream vorticity component. It amounts to a spanwise momentum exchange which will deform the base velocity profile. In forced flow Klebanoff *et al.* [28] found that this transport warped the velocity profile ahead of transition. The effect of higher harmonics was not found to be significant.

Detailed measurements of finite disturbance effects on temperature and velocity profiles by Jaluria and Gebhart [6, 26] indicate that these flows highly favour a narrow band of frequency for amplification, even after the beginning of transition. Hieber and Gebhart [13] have collected all available data on the first local appearance of highly amplified oscillations, arising from 'natural' disturbances. In terms of the coordinates of the stability plane (i.e. β_r and G^* in Fig. 2) all of these

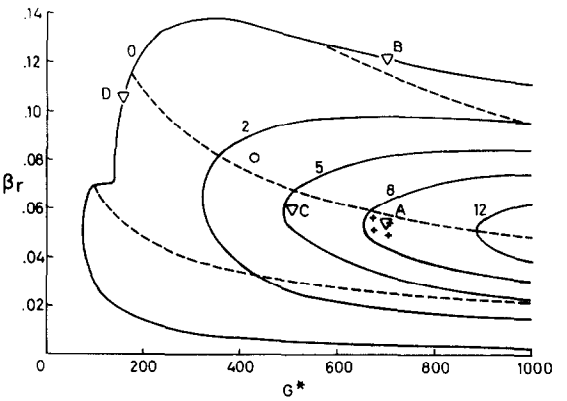

FIG. 2. Stability diagram from Hieber and Gebhart [13]—Contours of constant $-\frac{1}{4}\int \alpha_i \, dG$ for $Pr = 0.733$, $t_2^{(1)}(0) = 0$. Dashed curves are constant frequency paths. '∇' Points identifying the location of the present calculations. Data of highly amplified disturbances: '0' Eckert and Soehngen [14]: '+' Polymeropoulos [34].

data, in both air and water, lie in the portion of the unstable region which has the highest amplification rate. Ćolak-Antić [30] and Mollendorf and Gebhart [11], along with many other workers, have pointed out that such disturbances have a simple sinusoidal appearance even after being highly amplified. Thus we doubt that higher harmonics are of primary importance in the last stages preceding transition and will here consider only the mean secondary motion consequence of non-linear interaction. From (2) it is expressed as:

$$u_0^{(2)} = [\lambda^2 u_{01} \cos 2\theta z \, e^{-2(\alpha_{1i} x - \beta_{1i} \tau)} + \lambda\mu u_{02} \cos \theta \, e^{-(\alpha_{1i} + \alpha_{2i})x + (\beta_{1i} + \beta_{2i})\tau} + \mu^2 u_{03} e^{-2(\alpha_{2i} x - \beta_{2i} \tau)} + \lambda^2 u_{04} e^{-2(\alpha_{1i} x - \beta_{1i} \tau)}] \quad (7)$$

with similar expressions for the other flow components. The amplitude functions depend only on y and the subscript i refers to the imaginary part. The subscripts

01 and 02 identify respectively: (i) that part of the flow induced by the purely transverse component of the primary oscillation; (ii) the spanwise varying part of the flow induced by the transverse and two-dimensional components of the primary oscillation. Both the 01-flow and 02-flow vary in the spanwise direction and cause a spanwise distortion of the base velocity profile. The 03 and the 04 flows are merely two-dimensional distortions (no spanwise variation) generated by the two-dimensional and transverse primary oscillations, respectively.

The governing equations for the secondary mean flow are given in normalized form. Those for the 01-flow are:

Momentum:

$$2\alpha_{1i}(C_{1i}-F')\left[\frac{d^2}{d\eta^2}+4(\alpha_{1i}^2-\theta^2)\right]v_{01}+2\alpha_{1i}F'''v_{01}$$
$$-\frac{1}{G^*}\left\{\left[\frac{d^2}{d\eta^2}+4(\alpha_{1i}^2-\theta^2)\right]^2 v_{01}-2\alpha_{1i}\frac{dt_{01}}{d\eta}\right\}$$
$$=2\theta\frac{d\sigma_{01}^{(1)}}{d\eta}-2\alpha_{1i}\frac{d\sigma_{01}^{(1)}}{d\eta}-4(\alpha_{1i}^2-\theta^2)\gamma_{01}^{(1)}. \quad (8)$$

Energy:

$$2\alpha_{1i}(C_{1i}-F')t_{01}+v_{01}H'$$
$$-\frac{1}{PrG^*}\left[\frac{d^2}{d\eta^2}+4(\alpha_{1i}^2-\theta^2)\right]t_{01}=-\kappa_{01}^{(1)} \quad (9)$$

The y-vorticity component is

$$2\alpha_{1i}(C_{1i}-F')v_{01}-\frac{1}{G^*}\left[\frac{d^2}{d\eta^2}+4(\alpha_{1i}^2-\theta^2)\right]v_{01}$$
$$=-2\theta v_{01}F''-\frac{2\theta}{G^*}t_{01}+2\theta\lambda_{01}^{(1)}-2\alpha_{1i}\sigma_{01}^{(1)} \quad (10)$$

where

$$v_{01}=-2\theta u_{01}+2\alpha_{1i}w_{01}; \quad \text{and} \quad C_{1i}=\beta_{1i}/\alpha_{1i}.$$

The velocity components are

$$u_{01}=\frac{\alpha_{1i}}{2(\alpha_{1i}^2-\theta^2)}\frac{dv_{01}}{d\eta}+\frac{\theta}{2(\alpha_{1i}^2-\theta^2)}v_{01} \quad (11)$$

$$w_{01}=\frac{\alpha_{1i}}{2(\alpha_{1i}^2-\theta^2)}v_{01}+\frac{\theta}{2(\alpha_{1i}^2-\theta^2)}\frac{dv_{01}}{d\eta}. \quad (12)$$

The boundary conditions are

$$v_{01}(\infty)=0=v'_{01}(\infty)=v_{01}(\infty)=t_{01}(\infty)=v_{01}(0)$$
$$=v'_{01}(0)=v_{01}(0)=t_{01}(0). \quad (13)$$

Finally, the different forcing functions associated with the 01-flow may be expressed as:

$$\tilde{\lambda}_{01}^{(1)}=\frac{v^2G^{*5}}{(5x)^3}\lambda_{01}^{(1)}=\frac{vG^{*5}}{(5x)^3}\Big\{-2\alpha_{1i}u_1^{(1)}u_1^{(1)*}$$
$$+\frac{d}{d\eta}[\tfrac{1}{2}(u_1^{(1)}v_1^{(1)*}+u_1^{(1)*}v_1^{(1)})]$$
$$+(w_1^{(1)}u_1^{(1)*}+w_1^{(1)*}u_1^{(1)})\Big\} \quad (14)$$

and similar expressions for $\tilde{\gamma}_{01}^{(1)},\tilde{\sigma}_{01}^{(1)},\kappa_{01}^{(1)}$. The equivalent equations for the 02-flow are

Momentum equation:

$$(\alpha_{1i}+\alpha_{2i})(C_{2i}-F')\left\{\frac{d^2}{d\eta^2}+[(\alpha_{1i}+\alpha_{2i})^2-\theta^2]\right\}v_{02}$$
$$-\frac{1}{G^*}\left\{\frac{d^2}{d\eta^2}+[(\alpha_{1i}+\alpha_{2i})^2-\theta^2]\right\}^2 v_{02}$$
$$+(\alpha_{1i}+\alpha_{2i})v_{02}F'''=\frac{1}{G^*}(\alpha_{1i}+\alpha_{2i})\frac{d}{d\eta}t_{02}$$
$$+[\theta^2-(\alpha_{1i}+\alpha_{2i})^2]\gamma_{02}^{(1)}$$
$$+\frac{d}{d\eta}[\theta\sigma_{02}^{(1)}-(\alpha_{1i}+\alpha_{2i})\lambda_{02}^{(1)}]. \quad (15)$$

Energy equation:

$$(\alpha_{1i}+\alpha_{2i})(C_{2i}-F')t_{02}+v_{02}H'$$
$$-\frac{1}{PrG^*}\left[\frac{d^2}{d\eta^2}+(\alpha_{1i}+\alpha_{2i})^2-\theta^2\right]t_{02}=-\kappa_{02}^{(1)}. \quad (16)$$

The y-vorticity component is

$$(\alpha_{1i}+\alpha_{2i})(C_{2i}-F')v_{02}$$
$$-\frac{1}{G^*}\left[\frac{d^2}{d\eta^2}+(\alpha_{1i}+\alpha_{2i})^2-\theta)^2\right]v_{02}=-\theta v_{02}F''$$
$$-\frac{\theta}{G^*}t_{02}+\theta\lambda_{02}^{(1)}-(\alpha_{1i}+\alpha_{2i})\sigma_{02}^{(1)} \quad (17)$$

where $v_{02}=-\theta u_{02}+(\alpha_{1i}+\alpha_{2i})w_{01}$; and

$$C_{2i}=\frac{\beta_{1i}+\beta_{2i}}{\alpha_{1i}+\alpha_{2i}}.$$

The velocity components are

$$u_{02}=\frac{\alpha_{1i}+\alpha_{2i}}{(\alpha_{1i}+\alpha_{2i})^2-\theta^2}\frac{dv_{02}}{d\eta}+\frac{\theta}{(\alpha_{1i}+\alpha_{2i})^2-\theta^2}v_{02} \quad (18)$$

$$w_{02}=\frac{\alpha_{1i}+\alpha_{2i}}{[(\alpha_{1i}+\alpha_{2i})^2-\theta^2]}v_{02}+\frac{\theta}{[(\alpha_{1i}+\alpha_{2i})^2-\theta^2]}\frac{dv_{02}}{d\eta}.$$

The boundary conditions are

$$v_{02}(\infty)=0=v'_{02}(\infty)=v_{02}(\infty)=v_{02}(0)=v'_{02}(0)$$
$$=v_{02}(0)=t_{02}(0). \quad (19)$$

The appropriate forcing functions for the above are

$$\tilde{\lambda}_{02}^{(1)}=\frac{v^2G^{*5}}{(5x)^3}\lambda_{02}^{(1)}=\frac{v^2G^{*5}}{(5x)^3}$$
$$\times\Big[-(\alpha_{1i}+\alpha_{2i})2(u_2^{(1)}u_1^{(1)*}+u_2^{(1)*}u_1^{(1)})$$
$$+\frac{d}{d\eta}(v_1^{(1)}u_2^{(1)*}+u_1^{(1)*}v_2^{(1)}+u_2^{(1)}v_1^{(1)*}+v_2^{(1)*}u_1^{(1)})$$
$$+\theta(w_1^{(1)}u_2^{(1)*}+w_1^{(1)*}u_2^{(1)})\Big] \quad (20)$$

and similar expressions for $\tilde{\gamma}_{02}^{(1)}$, $\tilde{\sigma}_{02}^{(1)}$ and $\kappa_{02}^{(1)}$.

Equations (8–20) are the complete set for the spanwise-varying second order mean motion. Note that α and β have been assumed complex, allowing for both temporal and spatial growth factors. The use of

complex α and β may be seen to permit solutions to the transverse primary oscillation with longitudinal phase velocity and frequency identical to those of the two-dimensional primary wave, at identical values of G^*. The imaginary parts of both α and β may be regarded as individual terms of a total amplification factor. By Gaster's [31, 32] transformation these may be converted into either pure spatial or pure temporal form.

The principal characteristics we have calculated for the mean secondary flow may be shown in the form of streamlines. However, in our formulation, the three-dimensional and transient nature of the mean secondary flow does not lead directly to presentation of meaningful streamlines. This difficulty is avoided by two different approximations. First, for solutions which apply close to the neutral curve in the stability plane of Fig. 2 we assume that the mean secondary flow varies slowly in both x and τ, i.e. $e^{-\alpha_i x}$ and $e^{-\beta_i \tau} \simeq 1$. If one substitutes for x the wave length and for τ the period, the above approximations require that $\alpha_i/\alpha_r \ll 1$ and $\beta_i/\beta_r \ll 1$.

Second, for solutions which apply in the highly amplified region of the stability plane of Fig. 2 we will set $\alpha_i \equiv 0$ for the primary oscillation itself, and consider both the transverse and two-dimensional disturbances to be amplifying in time only. This procedure will, of course, for the solutions in this domaine result in different phase velocities for the two-dimensional and transverse primary waves. We assume that the error due to this difference in wave velocities is small. The error may in any event be kept within reasonable limits by restricting the maximum value of θ, the transverse wave number. In this way the difference in phase velocities may be kept less than perhaps ten percent [29]. The physical consequences of two different phase velocities are that the 02-flow would have a long standing wave (in x) of wave length $2\pi/(\alpha_{r1} - \alpha_{r2})$ and the 02-flow would reverse itself in five or six wave lengths. Experiments have not detected this effect (see Fig. 1).

The two remaining flow components, i.e. the 03 and 04-flow, are constant across the span. Neither of these flows contributes to any longitudinal roll system and since this is the main concern of the present investigation, they are not considered in any further detail [29].

Secondary mean flow streamlines

The solution to the mean secondary flow will be presented in the form of projected streamlines, formed by the transverse and the normal velocity components. For the temporarily amplifying flows these streamlines will apply formally only to a particular instant of time. The differential equation for the streamlines is

$$\frac{v_0^{(2)}}{w_0^{(2)}} = \frac{\mathrm{d}y}{\mathrm{d}z} \rightarrow$$

$$\frac{\mathrm{d}y}{\mathrm{d}z} = \frac{\lambda^2 e^{2\beta_{1i}\tau} \cos 2\theta z v_{01} + \lambda\mu e^{(\beta_{2i}+\beta_{1i})\tau} \cos \theta z v_{02}}{\lambda^2 e^{2\beta_{1i}\tau} \sin 2\theta z w_{01} + \lambda\mu e^{(\beta_{2i}+\beta_{1i})\tau} \sin \theta z w_{02}}.$$

Along a streamline we have

$$\frac{\lambda'^2}{2\theta} v_{01} \sin 2\theta z + \frac{\mu'\lambda'}{\theta} v_{02} \sin \theta z = \text{constant}. \quad (21)$$

NUMERICAL METHODS

Primary disturbance

The eigenvalue problem posed by the transverse and two-dimensional disturbance components is a sixth order system of linear homogeneous equations with variable coefficients. Nachtsheim [33] has shown that they possess three linearly independent solutions in the far field. Hieber and Gebhart [13] presented an integration technique for solving them which is significantly simpler than methods previously employed. Starting the solution from the far field and integrating the three linearly independent eigenfunctions separately, they only needed to employ two initial guesses. We used this scheme.

One may state the eigenvalue problem as

$$f(\alpha, \beta, \theta, Pr, G^*) = 0 \quad \text{at} \quad \eta = 0. \quad (22)$$

The parameters are θ, Pr and G^* and a change of any one of these requires a new set of eigenvalues. A correct set is determined from one of the three complex boundary conditions. One may arbitrarily choose two of the four components of α and β and compute the remaining two.

Typically either α_r or β_i is set to zero. β_r is chosen as some positive value. Then α_r, β_i or α_r, β_i are found from the boundary conditions. As mentioned above solutions close to the neutral curve for the transverse disturbance ($\theta \neq 0$) are obtained with both α_i and β_i different from zero. α_r, β_r are then fixed at the values found for a two-dimensional oscillation at the same G^*. In the highly amplified domain solutions for the transverse disturbance are obtained with $\alpha_i \equiv 0$.

The mean secondary flow

The equations governing the mean secondary flow are two-point boundary value problems. One may integrate them either starting out from the surface or in toward it, from the far field. However, the inhomogeneous terms are very complicated, and numerical integration from the wall was chosen as the most practical approach. A fourth order Runge–Kutta method was used to generate the solutions. At each step in the integration the values of the appropriate forcing functions were evaluated from stored, numerical solutions of the primary oscillation.

We will discuss the general procedure in terms of v_{01}. The solution requires that some value be guessed at the wall. We guessed $v_{01}''(0)$ and $v_{01}'''(0)$. They were corrected by iteration until the outward marching solution satisfied the far field boundary conditions to within a prescribed error, say $10^{-3} \rightarrow 10^{-4}$, at some large value of η. This was repeated several times, each time moving the terminal point further out along the η-axis. Convergence was assumed when the values of $v_{01}''(0)$ and $v_{01}'''(0)$ did not change by more than 0.01%

as the terminal point was moved from one location to the next.

Streamline calculation

The final step in these calculations is the generation of secondary mean flow streamlines. Different streamlines were found from (21) by changing the value of the stream function. Regarding θz as the independent variable in (21), solutions to the equation were obtained by scanning for zeros at fixed values of η (i.e. v_{01} and v_{02}) and stream function.

The ratio μ/λ indicates the relative magnitude (strength) of two dimensional and transverse disturbances, since the amplitude functions are normalized to a nominal order of 1.0. Presumably, the natural disturbances to which a flow might be subject would vary greatly in the relative prominence of these two effects. We examined this question by considering the range of μ/λ from values much greater than 1.0 to zero, i.e. down to no two-dimensional primary disturbance.

All the above calculations were performed in double precision on an I.B.M. 360/65. Two different mesh sizes were used in integrating the disturbance functions, 0.01 for $\eta < 6$, and 0.02 for $\eta > 6$. For the streamline calculation the step size in θz was 0.01.

SOME SOLUTIONS

Calculations were made at four flow conditions having very different linear stability characteristics, for a Prandtl number of 0.733. The flow conditions chosen are shown on the two-dimensional disturbance stability plane in Fig. 2. Also shown are observed points of highly amplified disturbances which arise naturally in experimental systems. The points of Polymeropoulos [34] are clustered around $G^* = 700$ and $\beta_r = 0.055$. This was the motivation for making two calculations at $G^* = 700$, one, point A, in the most highly amplified domain ($\beta_r = 0.055$) and the other, point B, close to the neutral curve ($\beta_r = 0.121$). Another condition of high amplification, corresponding to $G^* = 500$ is chosen, at C, whereas D is at about the same physical frequency, but at the neutral condition. This selection of conditions tests the principal characteristics of two-dimensional disturbance propagation.

Selected results from the calculations are shown in Figs. 3–12. On the figures showing amplitude functions, vertical lines along the horizontal axis indicate the points of maximum velocity of the base flow and the position of the outer critical layer, i.e. the point where the wave speed of the two-dimensional primary disturbance is equal to the base flow velocity.

G equal to 700*

Of principal interest is the modification of the base velocity profile by the secondary mean flow, which results from the action of Reynolds stresses. This could strengthen (or weaken) the convection of base flow energy into disturbance energy and affect disturbance growth (Lin [35]).

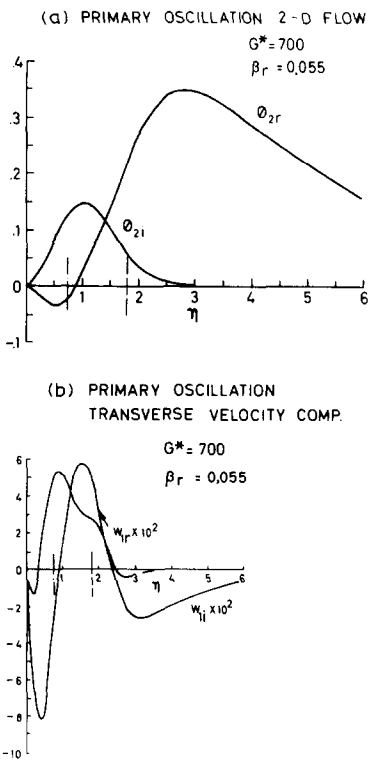

FIG. 3. For point A, the magnitude functions for the primary oscillation $\theta = 0.546$. — (a): $\alpha_r = 0.308$, $\beta_i = 0.00936$; — (b): $\alpha_r = 0.348$, $\beta_i = 0.00346$, $\theta = 0.564$; —·—: Location of $u_{max}^{(0)}$; ———: Location of criterical point.

Results for the highly amplified condition, point A, are considered first. The amplitude functions of the primary oscillations are shown in Fig. 3. Figure 4 indicates the magnitude of the functions v_{01}, w_{01}, v_{02},

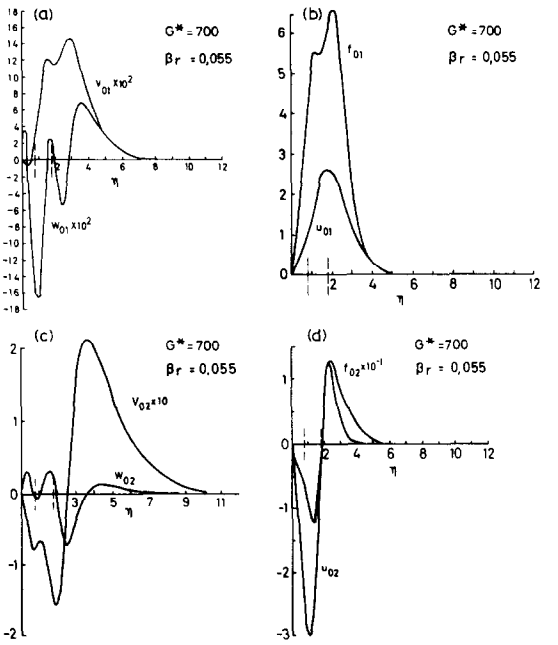

FIG. 4. For point A, the magnitude functions for the mean secondary flow. (a, b) 01-flow. (c, d) 02-flow. See caption to Fig. 3 for other flow parameters.

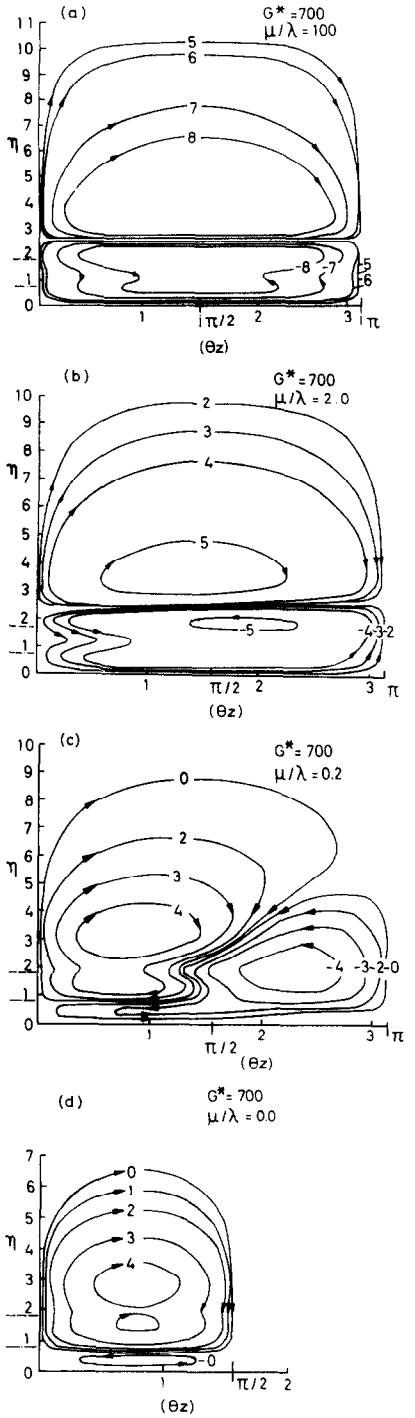

FIG. 5. For point A, the projected streamlines of the mean secondary flow. Stream function value: 0, 0.00005; 1, 0.0001; 2, 0.0002; 3, 0.0005; 4, 0.001; 5, 0.005; 6, 0.01; 7, 0.05; 8, 0.1. See caption to Fig. 3 for other flow parameters.

and w_{02}. These results are collected in an interpretation in streamlines in Fig. 5(a–d). These projected streamlines were generated with equation (21).

When $\mu/\lambda \gg 1$ we expect that the mean secondary flow is essentially the 02-flow. This flow induces the mean cellular vortex structure motion seen in Fig. 5(a) with spanwise periodicity of $2\pi/\theta$.

For increasing three-dimensionality of the disturbance, i.e. decreasing μ/λ, the 01-flow contribution to the mean secondary flow becomes more prominent. The vortex structure for the extreme case of a purely transverse primary oscillation ($\mu/\lambda = 0$) is seen in Fig. 5(d). The spanwise period is π/θ.

For other values of μ/λ the pattern goes through various stages of development. Two of these are seen in Figs. 5(b) and (c). As μ/λ decreases from much greater than 1, the centers of the outer roll move toward spanwise locations $\theta z = 2n\pi$ whereas the centers of the inner roll are pushed towards spanwise locations $\theta z = (2n+1)\pi$. These centers also move somewhat closer to the outer critical layer.

Such secondary motions imply a large momentum transport across the boundary region. Recall that the base velocity profile for this flow has a maximum located fairly close to the surface, i.e. at $\eta = 0.8$, and an inflection point in the outer part of the boundary layer, at $\eta \simeq 2$.

Consider the highly amplified circumstance which resulted in Fig. 5(a). Since we expect the flow prior to transition to be mainly two-dimensional, this 02-flow is of primary interest. The striking feature of this secondary mean flow is the presence of both an inner and outer longitudinal vortex roll. This is in contrast to the forced flow circumstance, where only a single eddy was found [23]. At $\theta z = (2n+1)\pi$ the inner roll carries high (and some low) momentum fluid from the inner part of the boundary layer to the outer slower-moving region. The counter-rotating outer vortex brings low momentum fluid from the far field into the boundary region at this same z-location. Note that at locations $\theta z = (2n+1)\pi$ the spanwise value of $u^{(1)}$ is at a minimum, see (2).

The sketches in Figs. 6 and 7 describe the consequences of these cross-flows The orientation and qualitative location of the two rolls, with respect to the base flow $u^{(0)}$, are seen in Fig. 6. The resulting modifications of the mean velocity profile are sketched in Fig. 7, for the two extreme locations in z. The secondary longitudinal velocity components u_{02} in Fig. 4(d) was used to infer these effects. Consider the modifications of the mean velocity profile at $\theta z = (2n+1)\pi$ and, recalling that the energy transfer to a disturbance is proportional to the velocity gradient of the mean flow [35], we see that disturbance growth may indeed be strongly augmented. The potential for the formation of a "shear-layer" is also present in this natural convection circumstance. At locations $\theta z = 2n\pi$ the vortex rolls have the opposite effect. The velocity maximum of the mean flow moves closer to the surface and the velocity gradient in the outer part of the boundary layer is reduced. This suggests a reduction in the disturbance growth rate.

Thus the mean secondary flow produces an alternate spanwise steepening and flattening of the outer part of the mean velocity profile. Another consequence is an alternating thinning and thickening of the boundary layer in the spanwise direction.

The above interpretation is somewhat modified if one

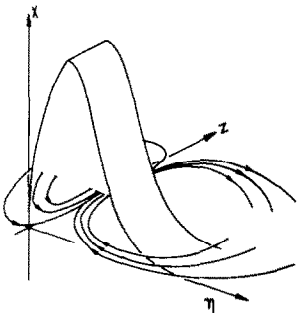

FIG. 6. For point A, the projected streamlines associated with the spanwise alternating mean secondary flow.

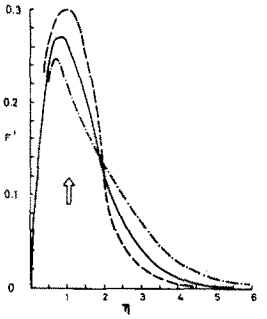

FIG. 7. For point A, the inferred qualitative distortions of the base flow profile for highly amplifying disturbances. ———: Spanwise location $\theta z = (2n+1)\pi$; —·—: Spanwise location $\theta z = 2n\pi$; ———: Base flow profile.

also considers the longitudinal vorticity component of the primary oscillation. This oscillation is periodic in x and has the same spanwise period as the 02-flow. Recall that

$$w_r^{(1)} = (w_{1r}^{(1)} \cdot \cos(\alpha_r x - \beta_r \tau) - w_{1i}^{(1)} \sin(\alpha_r x - \beta_r \tau)) \sin \theta z.$$

From Fig. 3(b) the effect of the oscillatory longitudinal vorticity component of the primary wave is seen to intensify the secondary circulation where $(\alpha_r x - \beta_r \tau) = (2n+1)\pi$. For an observer moving with the wave, this corresponds to the concave part of the streamline.

Since we are dealing with buoyancy driven flows it is of interest to assess the effect these longitudinal vortex rolls have on the mean temperature distribution. The modifications of the mean temperature distribution across the boundary layer are seen in Fig. 8. The secondary temperature distribution t_{02} in Fig. 4(d) was used to determine these distortions. The longitudinal vortex rolls apparently may produce an alternating spanwise reduction and augmentation of the local heat transfer. If so, moderation of the heat transfer (in terms of the local Nusselt number) should take place at spanwise locations $\theta z = (2n+1)\pi$, where we recall that conditions are favorable for most rapid growth of the velocity disturbance. At this spanwise location the primary temperature disturbance $t^{(1)}$ is at a minimum. For a surface of limited internal conduction this spanwise variation would produce an additional mode or mechanism which might be very important in determining stability.

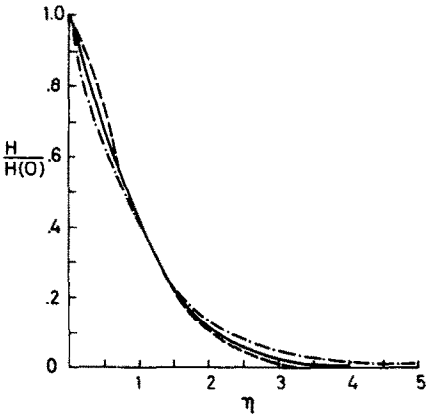

FIG. 8. For point A, the inferred qualitative distortions of flow temperature profile. ———: Spanwise location $\theta z = (2n+1)\pi$; —·—: Spanwise location $\theta z = 2n\pi$; ———: Base flow profile.

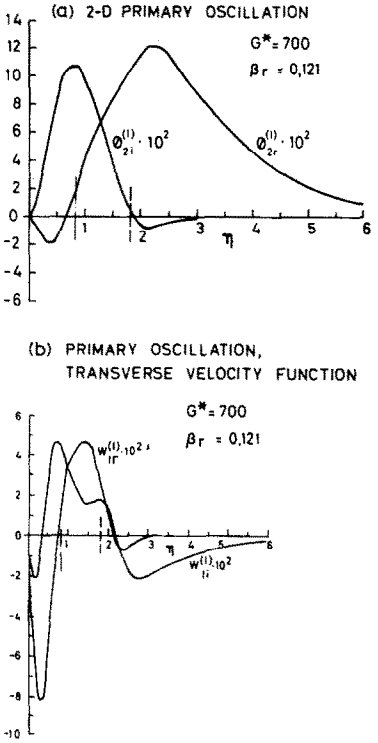

FIG. 9. For point B, the magnitude functions for the primary oscillation; $\alpha_r = 0.769$. —(a): 02-flow; $\alpha_i = -0.000897$; — (b): 01-flow; $\alpha_i = -0.0126$, $\beta_i = -0.00469$, $\theta = 0.348$; —·—: Location of $u_{\max}^{(0)}$; ———: Location of the critical point.

We now consider the results for point B on Fig. 2. Primary oscillation amplitude functions are shown in Fig. 9 and resulting longitudinal vortices are shown in Fig. 10, for three values of μ/λ. Here again $\mu/\lambda \gg 1$ is primarily a two-dimensional disturbance and μ/λ decreasing simulates increasing three-dimensionality. These results are very different from those at point A. Only a single longitudinal roll results.

In Fig. 10(c) is shown the longitudinal vortex produced by a purely transverse oscillation. At spanwise positions $\theta z = 2n\pi$ and $\theta z = (2n+1)\pi$ this system

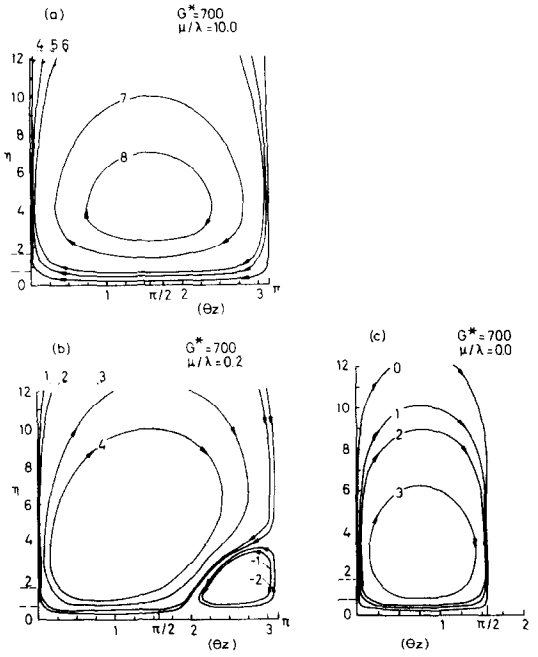

FIG. 10. For point B, the projected streamlines of the mean secondary flow. Stream function value: 0, 0.0001; 1, 0.0005; 2, 0.001; 3, 0.005; 4, 0.01; 5, 0.05; 6, 0.1; 7, 0.5; 8, 1.0. See caption to Fig. 9 for other flow parameters.

of vortices alternately reinforces and weakens the vortices induced by the 02-flow (Fig. 10a). A particular example of increased three-dimensionality is seen in Fig. 10(b) ($\mu/\lambda = 0.2$). The vortex rolls have been pushed towards spanwise positions $\theta z = 2n\pi$ and additional vortices appear at spanwise location $\theta z = (2n+1)\pi$.

The resulting modification of the mean flow, caused by the 02-flow of Fig. 10(a), is compatible with the former results. Spanwise locations $\theta z = (2n+1)\pi$ experience a momentum defect in the inner and outer part of the boundary layer. At $\theta z = 2n\pi$ the situation is reversed. Thus there is again an alternating spanwise thinning and thickening of the boundary layer. However, this single roll system does not appear to produce any spectacular or important steepening of the outer part of the velocity profile. The profile merely shifts in and out from the surface while retaining its original form. These changes would not be expected to augment disturbance growth.

The computed results for point C were in complete agreement with those discussed above for point A [29]. This is not surprising since both points lie in the highly unstable region and close to the path of fastest amplification. The main reason for making this calculation was to determine the secondary mean flow pattern over a wide range of Grashof numbers at essentially a constant frequency. The calculated results would be much less persuasive if the spatial form of the vortex system altered appreciably downstream (in x or G^*) for a given physical disturbance frequency. That would imply the omission of additional disturbance effects of an order comparable to those included.

Point D lies near the neutral curve and along the same high amplification path, see Fig. 2. Although we did not

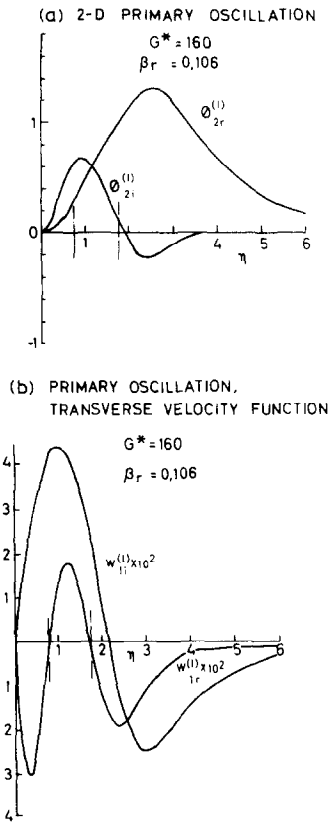

FIG. 11. For point D, the magnitude functions for the primary oscillation: $\beta_r = 0.106$; $\alpha_r = 0.670$. — (a): $\alpha_i = -0.0028$; — (b): $\alpha_i = 0.0516$, $\beta_i = 0.0049$, $\theta = 0.34$; —·—: Location of $u^{(0)}_{max}$; ———: Location of the critical point.

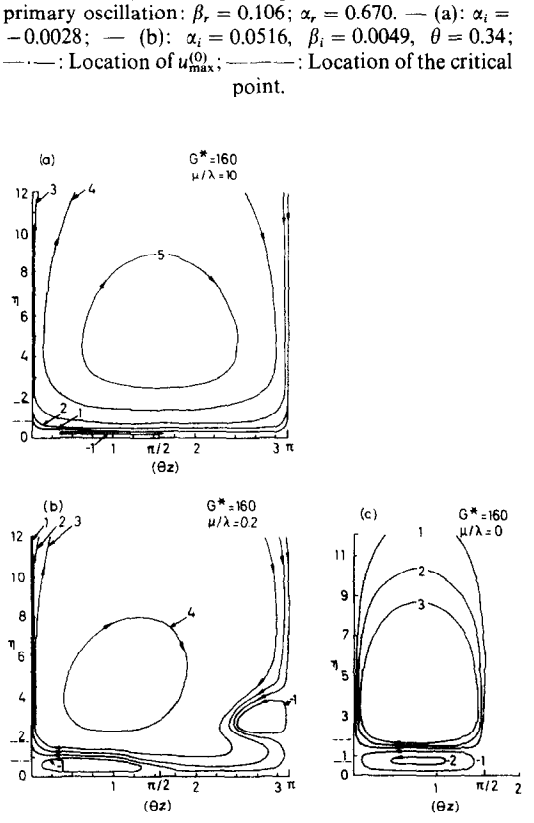

FIG. 12. Point D. Projected streamlines of the mean secondary flow. Stream function value: 1, 0.5×10^{-4}; 2, 0.5×10^{-3}; 3, 0.5×10^{-2}; 4, 0.5×10^{-1}; 5, 0.2. See caption to Fig. 11 for other flow parameters.

expect high amplification here, any mean secondary flow, in its earliest stages, would be interesting.

Primary oscillation amplitude distributions are shown in Fig. 11. The projected streamlines of the mean secondary flow are seen in Fig. 12, again for three values of μ/λ. The results, for the 02-flow in Fig. 12(a), for $\mu/\lambda = 10$, show one dominating outer roll. But we also see the beginning of a weak inner circulation. As before, the transverse wave number is $\theta = 2\pi/z$. For the purely spanwise oscillating disturbance, i.e. for $\mu/\lambda = 0$, the projected streamlines in Fig. 12(c) show both an inner and outer vortex, as for the highly amplified flows. Another stage of three-dimensionality, $\mu/\lambda = 2$, is seen in Fig. 12(b). The general behavior is the same as for the previous calculations.

This is particularly interesting and adds some additional weight to the present formulation since the calculations at D were carried out with identical frequency and wavenumbers for the two-dimensional and three-dimensional primary disturbance (i.e. both α and β complex).

COMPARISON WITH AVAILABLE DATA

There is considerable qualitative and quantitative evidence that secondary mean flow vortices immediately precede the disruption of highly disturbed laminar flow. Ćolak-Antić [30] suspended highly reflective aluminum particles in water and observed their behaviour during transition in the convection layer formed adjacent to a heated vertical flat surface. Two longitudinal vortices were seen, one near the surface and the other farther out, in accord with our results. He also studied disturbance behaviour and transition phenomena adjacent to an isothermal vertical surface in air. Both smoke filaments and hot wire anemometry were employed. Hot wire measurements were made at $G^* \approx 575$.

The conclusions, based upon both the observations in water and air were: (i) Three-dimensional effects occur almost simultaneously with the first observations of sinusoidal disturbances. (ii) Secondary mean flow longitudinal vortices exist both in air and in water. They occurred spontaneously at various points across the span. (iii) "Horse-shoe" shaped vortex loops were found. It was concluded that this was not the primary reason for breakdown. (iv) Intense shear layers within the boundary region were inferred from visual observations, although no details were given except that the inferred shear layers in general were said to be associated with the longitudinal eddies.

Warner and Arpaci [36] studied natural convection flow along a vertical flat plate in air. For conditions of incipient transition ($G^* \approx 600$) they found the local heat transfer rate and Nusselt number to decrease. On the average, incipient transition may be associated with the fastest amplifying disturbance. Our results suggest a decrease in the local Nusselt number at spanwise positions of maximum disturbance growth.

They also made detailed measurements of temperature distributions across the boundary layer, as tabulated by Warner [37]. In Fig. 13 we show these

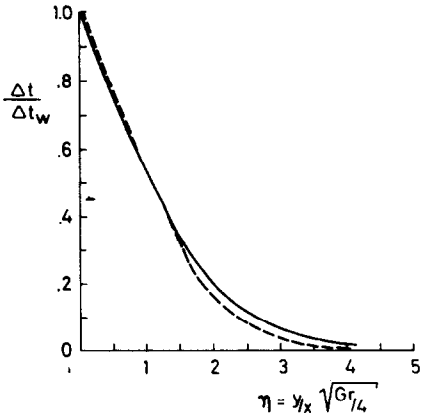

FIG. 13. Experimental observation of the distortion of the base flow temperature profile in an early stage of transition. Data: ——— Temperature profile for $Gr_x = 0.9 \times 10^9$, Warner [37]; ——— Calculated undisturbed laminar temperature profile (Sparrow and Gregg [27]).

data for the lowest transition Grashof number observed, $Gr_x = g\Delta t_w x^3/\nu^2 = 0.9 \times 10^9$ $(G^* = 600)$, where Δt_w is the temperature difference across the boundary layer. Also shown is the distribution for the undisturbed laminar flow. Both curves are plotted against the similarity variable $\eta = (y/x)\cdot\sqrt[4]{(Gr_x/4)}$. Warner's curve shows a general distortion in accord with the conjecture from our results at the spanwise location of fastest disturbance growth. Although the above comparisons are rough and qualitative and certainly not decisive, the trends are the same.

Our results indicate that spanwise steepening of the mean velocity profile occurs in the outer part of the boundary layer (Fig. 7). The maximum disturbance energy, or amplitude, should consequently also be found there. The results of Holman *et al.* [38] and of Polymeropolous and Gebhart [3] are particularly revealing in this aspect of disturbance growth. Holman found the maximum energy of the disturbance to be approximately half way through the boundary layer, i.e. at $\eta = 2$. Polymeropolous and Gebhart found the maximum amplitude of the disturbance to be at about the same location.

However, the most conclusive evidence of the relevance and role of a double longitudinal secondary mean flow vortex system as the consequence of non-linear interactions at larger downstream disturbance amplitudes, as well as the harbinger of eventual turbulence, are the experimental studies in water of Jaluria and Gebhart [6, 26]. This is seen first; in their observations of downstream amplification and non-linear interaction of introduced and controlled three-dimensional disturbances and, second; in their observations of disturbance forms which immediately precede the appearance of turbulent bursts in a flow subject to only naturally occurring disturbances.

The spatial, frequency and amplitude control in the first experiments permitted both the localization of the first appearance of non-linear growth in the periodic disturbance components and the detailed mapping of resulting secondary mean flows. We reproduce here

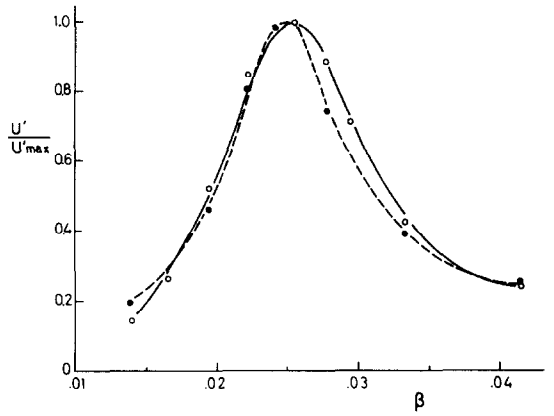

FIG. 14. Measured variation of downstream disturbance amplitude as a function of vibrator frequency. Data: ○, at the spanwise location of primary disturbance maximum; ●, at the spanwise location of primary disturbance minimum.

some data taken at $G^* = 530$, in an order which corroborates, with Fig. 1, the mechanisms assumed for and resulting from this analysis.

First, in Fig. 14, we see the measured amplitude of the longitudinal periodic disturbance component $u_2^{(1)}$, normalized by its maximum value, plotted as a function of input disturbance frequency β, the vibrator amplitude being constant. The maximum value occurs at $\beta = 0.025$, independent of spanwise location and, therefore, of the amplitude of the transverse disturbance. The frequency predicted by linear theory for two-dimensional disturbances, Hieber and Gebhart [13], at $G^* = 530$ is about 0.027. This condition, $G^* = 530$, is measured to be in the non-linear range. Thus, neither transverse disturbances nor non-linear amplification at first cause any appreciable change in the sharp frequency filtering characteristics of these flows.

Figure 15 shows the variation of measured transverse (in z) secondary mean flow component, w, normalized by the measured base flow maximum velocity $u_{max}^{(0)}$, across the boundary region, i.e. in η. Since w must be zero at $\eta = 0$, a double longitudinal mean flow vortex system has clearly been generated, through interaction with the transverse disturbance which, by Fig. 1, has the same propagation velocity as does the two dimensional disturbance. We note further the similarity of this distribution with the functions w_{01} and w_{02} calculated here as components of w and plotted in Fig. 4 for point A.

Figure 16 shows mean longitudinal velocities u, measured at a spanwise maximum and minimum of $u_2^{(1)}$, compared with u measured in the absence of introduced disturbances. These consequences follow directly from both calculated and measured w and also agree with the inferences of the present calculations drawn in Figs. 6 and 7.

We also note here that these experimental results are in close agreement with the measurements of w by Jaluria and Gebhart [6] of flows, preceding transition, into which no artificial disturbances had been introduced. However, no such complete results as those of Figs. 15 and 16 were obtained due to the randomness

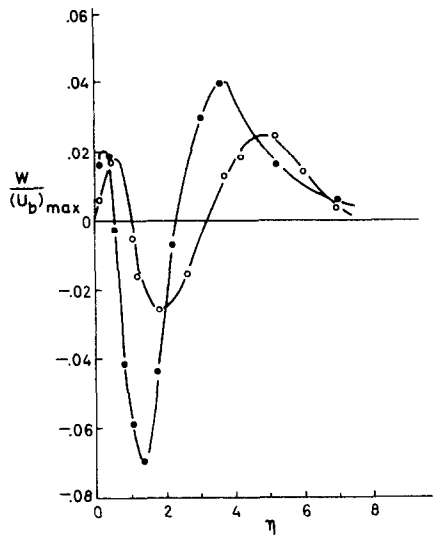

FIG. 15. Measured variation of the transverse component of the secondary mean flow at $G^* = 530$. Data: ●, at a spanwise location midway between locations of primary disturbance maximum and minimum amplitudes; ○, at 20% of the transverse wavelength from the above location toward the location of primary disturbance amplitude maximum.

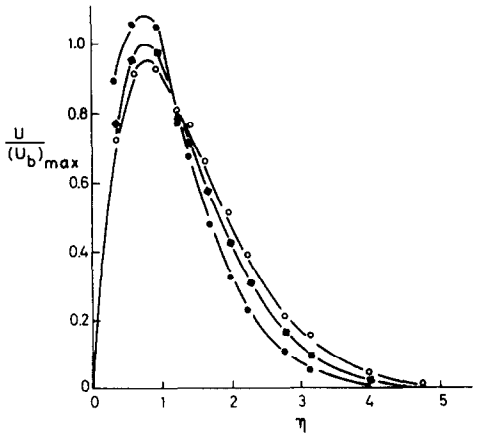

FIG. 16. Measured longitudinal mean flow profiles, compared with that for undisturbed flow. Data: ●, at spanwise location of primary disturbance minimum; ○, at spanwise location of primary disturbance maximum; ■, undisturbed flow.

of the disturbances and the high relative noise level of the instrumentation in this circumstance.

We may safely say, therefore, that measurements indicate a mechanism reasonably modelled by the present analysis. An intense shear layer is perhaps instrumental in the breakdown and transition processes in forced flow. The results of Ćolak-Antić [30] and those of Jaluria and Gebhart [6, 26] suggest a similar mechanism for natural convection. Secondary circulations produce spanwise regions of high shear.

ADDITIONAL OBSERVATIONS

A mean secondary longitudinal double vortex system is generated by non-linear interaction of two-dimensional and transverse disturbances. At certain spanwise positions at particular phases of the primary

wave, this circulation redistributes longitudinal momentum in planes perpendicular to the undisturbed mean flow. The spanwise varying distortion of the mean velocity profile increases downstream. Local steepening occurs at spanwise locations where the primary disturbance is at a spanwise minimum.

These calculated locations of highest shear are just the opposite of those found in analogous forced flow. The quiescent far field, rather than the region near the surface, is the source of the low momentum which causes the high shear region. We recall that the Görtler–Witting [39] theory, originally developed for forced flow, postulates that maximum intensification of secondary longitudinal vortices occurs where the streamline is concave. Thus, if the Görtler–Witting phenomenon has any significance in natural convection, it may further strengthen the effects calculated here.

One of the most significant features of our results is the critical dependence of the form of the non-linearly generated secondary mean flow on the base flow and frequency conditions, G^* and β, for which they were calculated. The points chosen for calculation sample the typical stability conditions predicted by linear analysis for a purely two-dimensional disturbance, i.e. neutral flows at both low and high G^*, D and B, highly amplifying flows at moderate and high G^*, C and A.

For B, only a single vortex arises and it does not produce a strong shear layer formation. At D, however, a second but much smaller eddy is found near the wall. Since D is located on the most highly filtered frequency path to C and A, where a strong double vortex system was found, it might appear that the double vortex system develops as the amplifying disturbance is convected downstream. This indicates that the secondary mean flow configuration need not appreciably change as the disturbance system is convected downstream, but that it enhances itself. We think that it is likely to be very important that this occurs simultaneously with the continued concentration of disturbance energy into the filtered two-dimensional primary wave. That is, the linear and non-linear mechanisms appear to proceed hand-in-hand and highly filtered. It would be very interesting to calculate the integrated effect of an initially three-dimensional disturbance along the filtered path and compare the results with the new data on disturbance form and transition.

Acknowledgements—The authors wish to acknowledge the support of the National Science Foundation through research grant GK 18529. The first author also wishes to acknowledge support from the "Royal Norwegian Council for Scientific and Industrial Research". We are also thankful for the helpful suggestions from Dr. S. F. Shen and for the data of Figs. 1 and 14–16 supplied by Mr. Yogesh Jaluria.

REFERENCES

1. G. B. Schubauer and H. K. Skramstad, Laminar-boundary layer oscillations and transition on a flat plate, NACA Dept. No. 909 (1948).
2. R. P. Dring and B. Gebhart, A theoretical investigation of disturbance amplification in external laminar natural convection, *J. Fluid Mech.* **34**, 551 (1968).
3. C. E. Polymeropoulos and B. Gebhart, Incipient instability in free convection laminar boundary layers, *J. Fluid Mech.* **30**, 225–239 (1967).
4. C. P. Knowles and B. Gebhart, An experimental investigation of laminar natural convection boundary layers, in *Progress in Heat and Mass Transfer*, Vol. 2, pp. 99–123. Pergamon Press, Oxford.
5. F. Godaux and B. Gebhart, An experimental study of the transition of natural convection flow adjacent to a vertical surface, *Int. J. Heat Mass Transfer* **17**, 93 (1974).
6. Y. Jaluria and B. Gebhart, On transition mechanisms in vertical natural convection flow, *J. Fluid Mech.* **66**, 309–337 (1974).
7. L. Pera and B. Gebhart, On the stability of laminar plumes: some numerical solutions and experiments, *Int. J. Heat Mass Transfer* **14**, 975–984 (1971).
8. L. Pera and B. Gebhart, On the stability of natural convection boundary layer flow over horizontal and slightly inclined surfaces, *Int. J. Heat Mass Transfer* **16**, 1147–1163 (1962).
9. B. Gebhart, Natural convection flow, instability and transition, *J. Heat Transfer* **91C**, 293 (1969).
10. B. Gebhart, Instability, transition and turbulence in buoyancy induced flows, *Ann. Rev. Fluid Mech.* **5**, 213 (1973).
11. J. C. Mollendorf and B. Gebhart, An experimental study of vigorous transient natural convection, *J. Heat Transfer* **92C**, 628–634 (1970).
12. G. S. H. Lock and F. J. Trotter, Observations on the structure of a turbulent free convection boundary layer, *Int. J. Heat Mass Transfer* **11**, 1225 (1968).
13. C. A. Hieber and B. Gebhart, Stability of vertical natural convection boundary layers: some numerical solutions, *J. Fluid Mech.* **48**, 625–646 (1971).
14. E. R. G. Eckert and E. Soehngen, Interferometric studies on the stability and transition to turbulence of a free-convection boundary layer, *Proc. Gen. Disc. Heat Transfer* 321–323 (1951).
15. E. R. G. Eckert, J. P. Hartnett and T. F. Irvine, Jr., Flow, visualization studies of transition to turbulence in free-convection flow, ASME Paper No. 60-Wa-260 (1960).
16. T. Fujii, On the development of a vortex street in a free-convection boundary layer, *Bull. J. S. M. E.* **2**(8), 551 (1959).
17. T. Fujii, M. Takeuchi, M. Fujii, K. Suzaki and H. Uehara, Experiment on natural convection heat transfer from the outer surface of a vertical cylinder to liquids, *Int. J. Heat Mass Transfer* **13**, 753–787 (1970).
18. A. A. Szewczyk, Stability and transition of the free-convection boundary layer along a flat plate, *Int. J. Heat Mass Transfer* **5**, 903 (1962).
19. F. R. Hama, J. D. Long and J. C. Hegarty, On transition from laminar to turbulent flow, *J. Appl. Phys.* **28**, 388 (1957).
20. P. Ćolak-Antić, Hitzdraht messungen des laminar-turbulenten Umsclags bei freier Konvektion, *Jb. WGLR* 172–176 (1964).
21. J. D. Benny and C. C. Lin, On the secondary motion induced by oscillations in a shear flow, *Physics Fluids* **3**, 656 (1960).
22. J. D. Benny, A non-linear theory for oscillations in a parallel flow, *J. Fluid Mech.* **10**, 209–236 (1961).
23. J. D. Benny, Finite amplitude effects in an unstable laminar boundary layer, *Physics Fluids* **7**, 319–326 (1964).
24. J. T. Stuart, Hydrodynamic stability, *Appl. Mech. Rev.* **18**, 523 (1965).
25. L. M. Hocking, K. Stewartson, J. T. Stuart and S. M. Brown, A nonlinear instability burst in plane parallel flow, *J. Fluid Mech.* **51**, 705–735 (1972).
26. Y. Jaluria and B. Gebhart, An experimental study of non-linear disturbance behaviour in natural convection, *J. Fluid Mech.* **61**, 337 (1973).
27. E. M. Sparrow and J. L. Gregg, Laminar free convection from a vertical plate with uniform surface heat flux, *J. Heat Transfer* **78C**, 435 (1956).

28. P. S. Klebanoff, K. D. Tidstrom and L. M. Sargent, The three-dimensional nature of boundary-layer instability, *J. Fluid Mech.* **12**, 1–34 (1961).
29. T. Audunson, Part I: An experimental and analytical study of natural convection with appreciable thermal radiation effects. Part II. Observations on the secondary three dimensional mean motion induced by oscillations in a natural convection boundary layer, Ph.D. Thesis, Cornell University (1971).
30. P. Colak-Antić, Dreidimensionale Instabilitatserscheinungen des laminar-turbulenten Umschlages bei freier Konvektion Längs einer vertikalen geheizhen Platte, *Sber. Heidelb. Akad. Wiss., Mathe.-natur Klasse* 315–416 (1962–64).
31. M. Gaster, A note on the relation between temporally-increasing and spatially-increasing disturbances in hydrodynamic stability, *J. Fluid Mech.* **32**, 222–224 (1962).
32. M. Gaster, The development of three-dimensional wave packets in a boundary layer, *J. Fluid Mech.* **32**, 173–184 (1967).
33. P. E. Nachtsheim, Stability of free-convection boundary layer flows, NASA TND-2089 (1963).
34. C. E. Polymeropoulos, A study of the stability of free-convection flow over a uniform flux plate in nitrogen, Ph.D. Thesis, Cornell University (1966).
35. C. C. Lin, *The Theory of Hydrodynamic Stability*. Cambridge University Press, London (1955).
36. C. Y. Warner and V. S. Arpaci, An experimental investigation of turbulent natural convection in air at low pressure along a vertical heated plate, *Int. J. Heat Mass Transfer* **11**, 397 (1968).
37. C. Warner, Turbulent natural convection in air along a vertical flat plate, Ph.D. Thesis, The University of Michigan (1966).
38. J. P. Holman, H. E. Gartrell and E. E. Soehngen, An interferometric method of studying boundary layer oscillations, *J. Heat Transfer* **82C**, 263–264 (1960).
39. H. Görtler and H. Witting, Theorie der sekundaren Instabilitat der laminaren Grenzschichten, in *Boundary Layer Research Symposium, Freiberg*, edited by H. Görtler, pp. 110–126. Springer, Berlin (1957).

MOUVEMENTS SECONDAIRES APPARAISSANT DANS UN ECOULEMENT EN CONVECTION LIBRE

Résumé—L'article présente une approche numérique du développement et de l'intéraction non linéaire entre perturbations bidimensionnelles et transversales dans une couche limite en convection naturelle adjacente à une paroi plane verticale. Il apparait que l'effet d'une amplitude finie se traduit par l'établissement d'un double système tourbillonnaire secondaire longitudinal. Pour certaines positions transversales, et pour des phases particulières de l'onde primaire, cette circulation longitudinale hautement organisée produit des épaississements et des amincissements alternés de la couche limite, se traduisant par des augmentations et des diminutions de la pente du profil de vitesse dans l'écoulement de référence. Des mesures de réponse de l'écoulement à des perturbations bidimensionnelles, controlées dans le sens de l'écoulement et modulées par une onde stationnaire transversale, présentent également des caractéristiques semblables et les caractères de deux perturbations demeurent en fait liés, présentant une faible différence de phase. Ainsi les conditions de la transition déterminées expérimentalement correspondent de très près à des écoulements dans lesquels la présente analyse découvre de larges mouvements tourbillonnaires.

MITTLERE SEKUNDÄRBEWEGUNGEN IN EINER AUFTRIEBSINDUZIERTEN STRÖMUNG

Zusammenfassung—Es wird eine numerische Berechnung angegeben über das Wachstum und die nichtlineare Einwirkung von zweidimensionalen und querwirkenden Störungen auf die Grenzschicht an einer senkrechten, ebenen Wand bei natürlicher Konvektion. Es ergab sich, daß die endlichen Amplitudeneffekte ein mittleres sekundäres Doppellängswirbelsystem liefern. In gewissen Spannweiten und für besondere Phasen der Primärwelle verursacht diese gut ausgerichtete Längszirkulation, abhängig von der Spannweite, abwechselnd eine Verdünnung oder Verdickung des Grenzschichtbereichs und daraus resultierend eine Erhöhung oder eine Abflachung der Profile der Grundströmungsgeschwindigkeit.

Messungen der Reaktion der Strömung auf kontrollierte zweidimensionale Störungen, moduliert durch eine stehende Querwelle, zeigen ähnliche Charakteristika und machen deutlich, daß die beiden Störungserscheinungen miteinander verbunden sind und auch verbunden bleiben bei kleinen Phasendifferenzen. Experimentell bestimmte Übergangsbedingungen korrespondieren somit sehr eng mit Strömungen, in denen sich nach dieser Analyse große Wirbelbewegungen finden.

ВТОРИЧНЫЕ ОСРЕДНЕННЫЕ ТЕЧЕНИЯ, ВОЗНИКАЮЩИЕ В СВОБОДНО-КОНВЕКТИВНОМ ПОТОКЕ

Аннотация — Представлены результаты численного расчета развития и нелинейного взаимодействия двух возмущений, пространственного и поперечного, в свободно-конвективном пограничном слое на вертикальной плоской пластине. Найдено, что возмущения конечной амплитуды приводят к образованию двойной системы продольных осредненных вторичных вихрей. При определенном направлении потока вдоль пластины и отдельных фазах основной волны эта продольная циркуляция вызывает попеременное увеличение или уменьшение толщины пограничной области, в результате чего происходит изменение крутизны профиля скорости основного потока. Аналогичные характеристики проявляются также и при определении реакции потока на регулируемые двумерные возмущения по потоку, вызванные поперечной стоячей волной. И действительно, обе характеристики возмущения тесно связаны между собой при небольшой разности фаз. Таким образом, экспериментально найденные условия перехода соответствуют условиям интенсивного вихревого движения, обнаруженного с помощью этого анализа.